RESEARCH



Flux Calibration of Coronal Magnetic Field

Marek Vandas¹ · Evgeny Romashets²

Received: 2 May 2024 / Accepted: 17 August 2024 © The Author(s) 2024

Abstract

Romashets and Vandas (2024) derived a method for the determination of Euler potentials at a spherical surface and applied it to the geomagnetic field. Here, we apply it to find Euler potentials at the source surface. A regular mesh defined by Euler potentials divides the source surface to surface elements with the same magnetic flux. By tracing magnetic-field lines away from the source surface, Euler potentials can be extended into the heliosphere.

Keywords Magnetic fields · Corona

1. Introduction

Spherical harmonic analysis was used for the description of the terrestrial magnetic field for centuries (Chapman and Bartels 1940). It has been shown that the method is applicable for the solar magnetic field (Chapman 1943). The actual application began much later (Newkirk and Altschuler 1969). Solar global open magnetic fields were studied with this technique in Levine, Altschuler, and Harvey (1977a,b) by tracing along the field lines from the source surface down to the photosphere. Multiple discrete regions of the open magnetic field in the photosphere were reported. The comparison of open magnetic field regions with observed coronal holes was done in Levine (1978). The source surface is commonly located at a distance of 2.5 solar radii. It is assumed that only the radial component of the solar magnetic field is present on it. At distances greater than 2.5 solar radii from the center of the Sun, the interplanetary magnetic field smoothly changes from a radial to a spiral one due to the solar rotation.

Recent spacecraft missions, such as SDO, STEREO, and PROBA 2 provide high-resolution magnetograms, which lead to a better understanding of the structure of the solar magnetic field. Magnetic synoptic observations along the line of sight during entire revolutions of the Sun allow us to reconstruct a magnetic field in the region between the photosphere and the source surface, by means of spherical harmonic analysis.

M. Vandas

vandas@asu.cas.cz

E. Romashets eromashets@lamar.edu

Published online: 29 August 2024

- Astronomical Institute of the Czech Academy of Sciences, Prague, Czech Republic
- ² Lamar University, Department of Physics, Beaumont, TX, USA



119 Page 2 of 9 M. Vandas, E. Romashets

We have recently developed a method for high-resolution α - β mapping of a magnetic field on a surface (Romashets and Vandas 2024); α and β are Euler potentials (Euler 1769). We apply it here for α - β mapping at the source surface. Equally spaced α and β contours divide a given surface into a large number of surface elements with equal magnetic flux through each element. This magnetic flux calibration can be done with a very high precision. Euler potentials offer an alternative to a direct usage of a vector magnetic field. Tasks, which are usually solved with Euler potentials, can also be solved with other methods. However, it is an advantage to have an alternative way, e.g., for verifications.

The observations of coronal holes show the position of the open field lines, but do not specify how fast the field lines expand and occupy most of the volume of the outer solar corona, that is, outside of the regions filled in by returning field lines. There were attempts to label each field line as R or NR, returning or non-returning, and to watch how much of the volume each kind occupies. Rapidly expanding coronal holes are maybe not as geo-effective as slowly expanding ones. In order to study the behavior of the magnetic-field lines from coronal holes, it is convenient to use a method of magnetic flux calibration, which divides a given surface into a large number of surface elements with equal magnetic flux through each element. The two-dimensional mesh labels each element with two numbers. The simplest version of the calibration uses only a normal component of the magnetic field on the surface and does not provide the mapping outside of the surface. The more time-consuming version of the calculation provides a two-dimensional mapping of the entire volume. It uses three components of the magnetic field in the entire volume. Once it is completed, the analysis of magnetic-field extension from each element of the area becomes easier, that is, monitoring where particular label sets go and at what speed. The flux calibration is the way of visualization of the expansion or contraction of the magnetic tubes in the volume. This is done well with the help of Euler potentials, if they are known.

It was concluded in Kononovich and Shefov (2013) and Ivanov and Kharshiladze (2006) that the solar cycle can be divided into two-year quasi cycles of the global open solar magnetic field (GOSMF), phases of GOSMF formation, minimum, growth, maximum, and decay. At the beginning of the minimum, growth, and maximum phases, the total magnetic flux through the source surface experiences a sudden decrease. During the minimum phase, the GOSMF rotates with respect to the Sun in the direction to the west, while the direction changes to the east during the growth phase. The maximum solar activity happens when the four-sector structure of the interplanetary magnetic field is replaced by the two-sector structure, and when regions of the open solar magnetic field are concentrated near a main active longitude (Vitinskii, Kopetskii, and Kuklin 1986). It seems that the key to understanding solar activity is in studying and modeling the open solar magnetic field. We may think that everything is determined by the rate of magnetic flux change as a function of distance from the Sun. If the rate of the open magnetic flux decrease with distance is very small, this may lead to increased activity in this region. To confirm this, one should calculate the flux and analyze its rate of change near the coronal holes.

Euler potentials are used to study behavior of magnetic fields (e.g., Sweet 1950; Dungey 1958), motion of energetic particles (e.g., Ray 1963), Alfvén waves (Webb et al. 2010), and in models of Earth's magnetosphere/ionosphere (e.g., Wolf et al. 2006; Schulz and Chen 2008; Zaharia 2008). There are not so many known Euler potentials for magnetic fields and they are mostly limited to simple fields, e.g., a dipole field (e.g., Schulz and Chen 2008), Alfvén waves (Webb et al. 2010), or Parker's interplanetary field (Webb et al. 2010). In this paper, we present a method on how to determine Euler potentials for a more complex field, much closer to a real field, that is, Euler potentials of a solar coronal field at the source surface. These Euler potentials are not determined numerically on a grid, but formulae with analytical functions are provided for them.



2. Method

Euler potentials α and β are two scalar functions reproducing the magnetic-field vector via

$$\mathbf{B} = \nabla \alpha \times \nabla \beta. \tag{1}$$

The α and β are constant along magnetic-field lines and the value $d\alpha d\beta$ is equal to the magnetic flux of the region defined by $d\alpha d\beta$. We use a spherical coordinate system, r, θ , and φ . Euler potentials are functions of all three coordinates in general. We search them at the source surface, $r = r_{ss}$, so we take them as functions of θ and φ only, $\alpha(\theta, \varphi) \equiv \alpha(r_{ss}, \theta, \varphi)$, $\beta(\theta, \varphi) \equiv \beta(r_{ss}, \theta, \varphi)$. **B** has only the B_r component at the source surface, and Equation 1 yields

$$B_r^{(E)} = B_r(r_{ss}, \theta, \varphi) = \frac{1}{r_{cs}^2 \sin \theta} \left[\frac{\partial \alpha(\theta, \varphi)}{\partial \theta} \frac{\partial \beta(\theta, \varphi)}{\partial \varphi} - \frac{\partial \alpha(\theta, \varphi)}{\partial \varphi} \frac{\partial \beta(\theta, \varphi)}{\partial \theta} \right]. \tag{2}$$

On the other hand, the magnetic field $(B_r^{(ss)}, 0, 0)$ at the source surface is given by harmonic coefficients g_{lm} and h_{lm} , following from observations (Hoeksema 1985)

$$B_r^{(ss)} = \sum_{l=0}^{9} (2l+1) \left(\frac{r_0}{r_{ss}}\right)^{l+2} \sum_{m=0}^{l} P_l^m(\cos\theta) (g_{lm}\cos m\varphi + h_{lm}\sin m\varphi), \tag{3}$$

where r_0 is the solar radius and P_l^m are associated Legendre polynomials.

The Euler potential α is assumed in the form

$$\alpha(\theta,\varphi) = r_{\rm ss}^2 \sqrt{B_0^2 - B_r^2(r_{\rm ss},\theta,\varphi)},\tag{4}$$

where B_0 is a free parameter ensuring a positive value at the square root and acceptable agreement between the B_r values at the source surface from Equations 2 and 3. It means that the B_0 is found by some trials.

The second Euler potential, β , is searched as

$$\beta(\theta,\varphi) = c_{00}\varphi + \sum_{n=1}^{N} c_{n0} P_n(\cos\theta) + \sum_{m=1}^{M} c_{0m} \cos m\varphi$$
$$+ \sum_{n=1}^{N} \sum_{m=1}^{M} P_n(\cos\theta) (c_{nm} \cos m\varphi + d_{nm} \sin m\varphi), \tag{5}$$

where P_n are the Legendre polynomials. The summation limits, N and M, are set similarly to B_0 , by trial and error. The coefficients, c_{nm} and d_{nm} , are found by a least square method minimizing the integral

$$\int [B_r^{(E)} - B_r^{(ss)}]^2 dS \tag{6}$$

over a selected region at the source surface. According to Equation 2, $B_r^{(E)}$ is a sum of terms multiplied by the coefficients. We insert the sum into the integral 6. The minimum condition means that each derivative of the integral by a coefficient must be zero. We subsequently differentiate the integral by the coefficients, set the result to zero, and at the end obtain a set of linear equations for the coefficients, which is easily solved.



119 Page 4 of 9 M. Vandas, E. Romashets

Figure 1 $B_r^{(ss)}$ as a function of solar latitude and longitude for the Carrington rotation 2194.

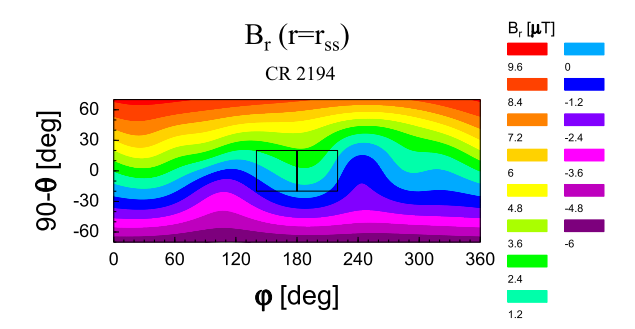
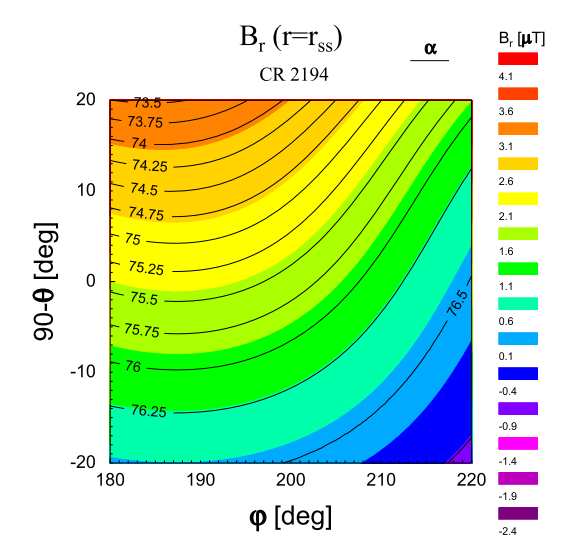


Figure 2 The α iso-lines for the right region, overlaying the $B_r^{(ss)}$ distribution.



3. Results

Figure 1 displays contours of the B_r component ($B_r^{(ss)}$) at the source surface for the Carrington rotation 2194 (16 August – 12 September 2017). In order to obtain an acceptable agreement between $B_r^{(ss)}$ and $B_r^{(E)}$, we have to limit it to a smaller region than drawn in the figure. We selected two adjacent regions, marked by rectangles in the figure, covering $40^\circ \times 40^\circ$. We call them left and right regions in the following text.

Figure 2 shows contours of α in the right region. It follows from Equation 4 that B_0 must be larger or equal to the maximum magnetic-field magnitude in the region, which is about 7 μ T in our case. We started with this value. When we increased B_0 several times, we observed that the model field became better (according to the integral 6). In such a way, we arrived at the value $B_0^2 = 150 \ \mu\text{T}^2$, which is used here. In addition, for the calculation of β , we put N = M = 21. The resulting β for the right region is shown in the next Figure 3. Using the obtained coefficients c_{nm} and d_{nm} , we can analytically calculate $B_r^{(E)}$ from Equation 2. The maximum relative difference between $B_r^{(\text{ss})}$ and $B_r^{(\text{E})}$ is of the order of 10^{-5} for the right region.

The same process is completed for Figures 4 and 5 in the left region. Now the maximum relative difference between $B_r^{(ss)}$ and $B_r^{(E)}$ is of the order of 10^{-4} .



Figure 3 The β iso-lines for the right region, overlaying the $B_r^{(ss)}$ distribution.

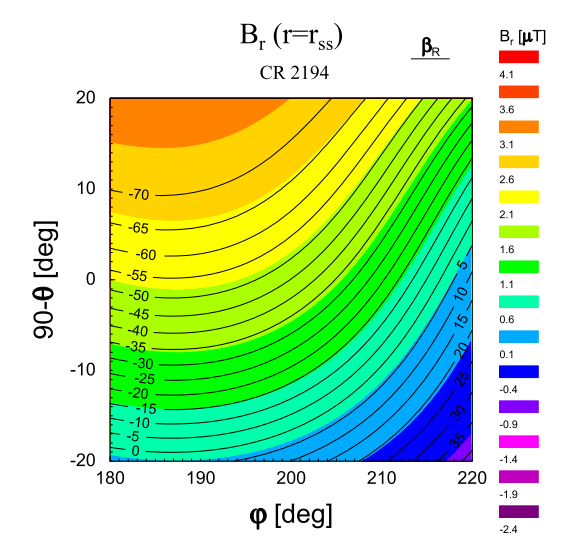
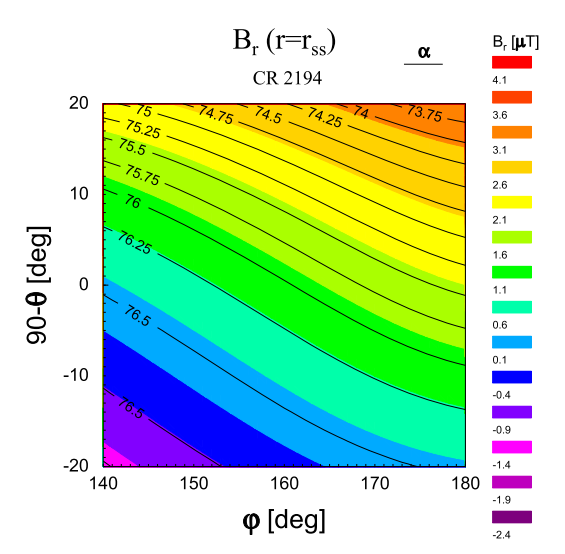


Figure 4 The α iso-lines for the left region, overlaying the $B_r^{(ss)}$ distribution.



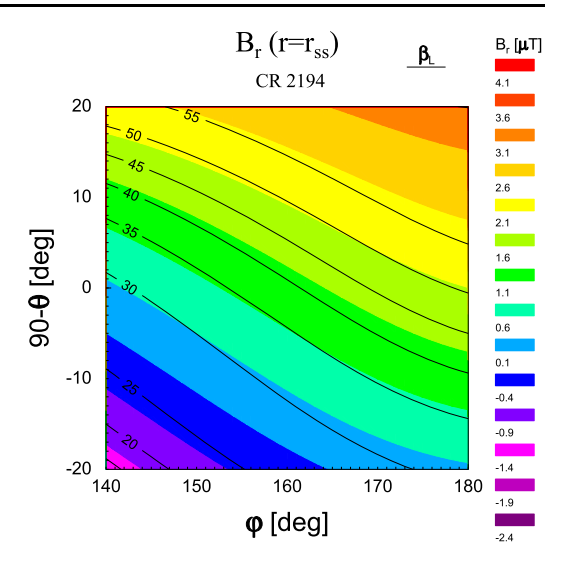
Consider both regions together. The function α is global (provided B_0 is the same, which is) and goes smoothly from one region to the other, as it is demonstrated in Figure 6. However, it is not true for the β . The coefficients were determined independently, so we have two different sets of them, and one cannot expect that betas will be smooth at the common boundary ($\varphi = 180^{\circ}$), see Figure 7. Therefore, we denoted β of the left and right regions as β_L and β_R , respectively.

There is a manner in how to find a common β for the both regions. That is, we modify β in the right region (β_R) to make it smooth through the joint boundary. One can easily verify, that when β fulfills Equation 1, then $\beta' = \beta + f(\alpha)$, where f is a function, fulfills it with the same α . Now consider α at the common boundary (see Figure 6). One can see it as a function of θ , $\alpha(\theta, \pi)$. If this function is monotonic (which in our case is), then an inverse function exists; we denote it $\theta_b(\alpha)$. The β for the both regions is: $\beta(\theta, \varphi) = \beta_L(\theta, \varphi)$ for



119 Page 6 of 9 M. Vandas, E. Romashets

Figure 5 The β iso-lines for the left region, overlaying the $B_r^{(ss)}$ distribution.



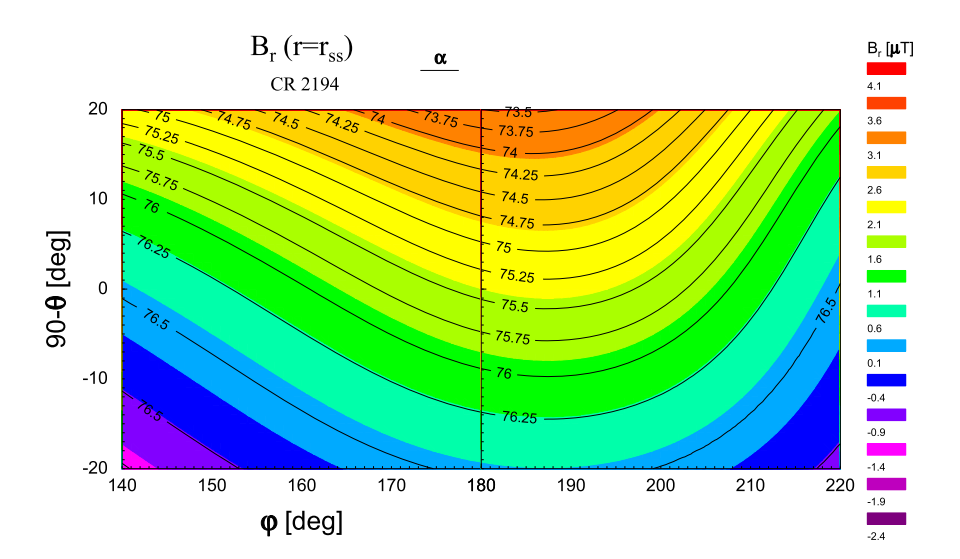


Figure 6 The α iso-lines for the both regions, overlaying the $B_r^{(ss)}$ distribution. These are Figures 2 and 4 one by one.

the left region, $\beta(\theta, \varphi) = \beta_R(\theta, \varphi) + \beta_L\{\theta_b[\alpha(\theta, \varphi)], \pi\} - \beta_R\{\theta_b[\alpha(\theta, \varphi)], \pi\}$ for the right region. This β is shown in Figure 8. At the common boundary, it fits well, see Figure 9. Using α and β , we numerically calculated B_r by Equation 1. Its distribution is shown in Figure 10. It matches the contours of the original $B_r^{(ss)}$ very well. The calculation involved numerical differentiation of α and β using a polynomial approximation.



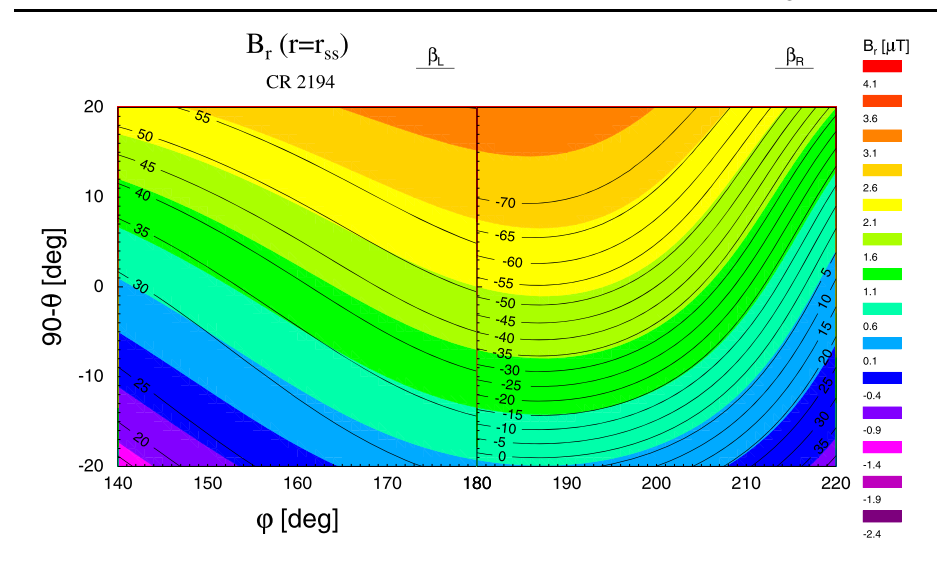
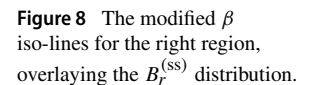
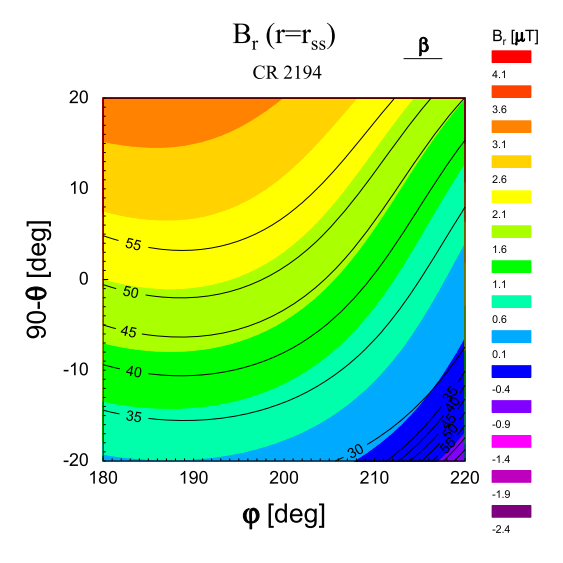


Figure 7 Figures 3 and 5 one by one demonstrating that β is discontinuous at the joint boundary.





4. Conclusions

We presented a method on how to determine Euler potentials α and β at the source surface. Equally spaced iso-contours of α and β at the source surface creates a mesh of equally distributed magnetic flux. Tracing along magnetic-field lines enables us to extend α - β mapping into the heliosphere and partly to the photosphere (to regions where the field is open), because α and β remain constant along the field lines. For the extension into the heliosphere, one needs a magnetic-field model (e.g., Romashets, Vandas, and Poedts 2007).

In order to keep numerical errors low, the determination of β was limited to a relatively small area of the source surface. We demonstrated a procedure where betas of these areas can be joined. It relies on the existence of a monotonic function, which is not always guaranteed.



119 Page 8 of 9 M. Vandas, E. Romashets

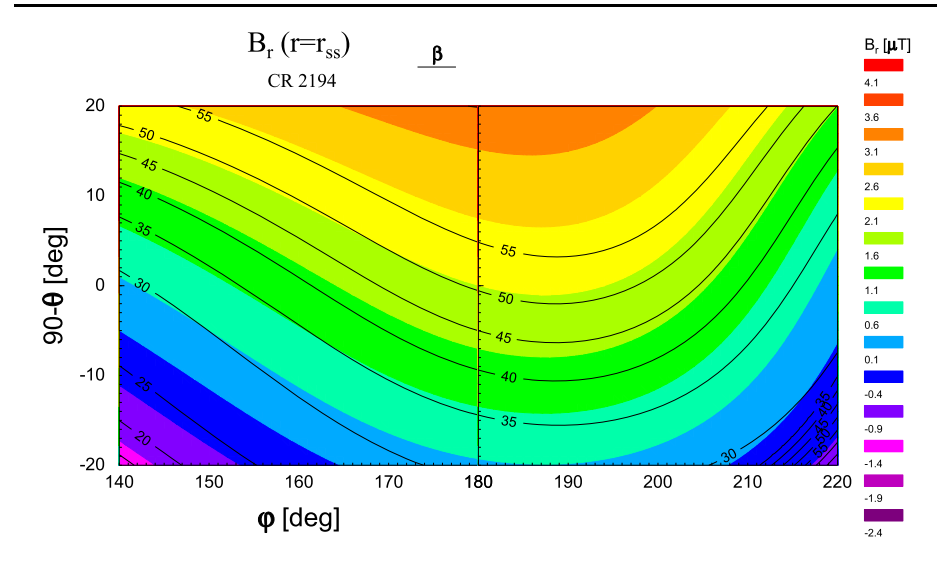


Figure 9 The β iso-lines for the both regions, overlaying the $B_r^{(ss)}$ distribution. These are Figures 5 and 8 one by one.

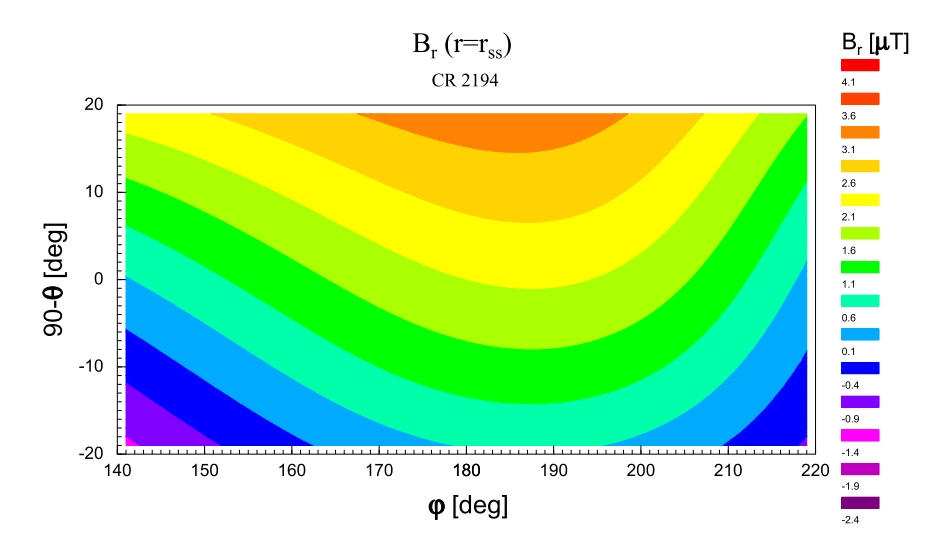


Figure 10 Contours of B_r at the source surface, obtained numerically from the final α and β .

We work on a modified method that overcomes this limitation and enables us to map larger areas and eventually the whole source surface.

Acknowledgements The harmonic coefficients for the Carrington rotation 2194 were taken from the Wilcox Solar Observatory (http://wso.stanford.edu, courtesy of J. T. Hoeksema). The Wilcox Solar Observatory is currently supported by NASA.

Author contributions E.R. suggested the method for alpha and beta determination, M.V. suggested the way of beta correction, and made calculations and figures, both authors wrote the text and made editing.



Funding Open access publishing supported by the National Technical Library in Prague. This work was supported by the NSF grant 2230363. M. V. acknowledges support from the AV ČR grant RVO:67985815 and the GA ČR grant 21-26463S.

Data Availability The harmonic coefficients for the Carrington rotation 2194 were taken from the Wilcox Solar Observatory (http://wso.stanford.edu, courtesy of J. T. Hoeksema).

Declarations

Competing interests The authors declare no competing interests.

Open Access This article is licensed under a Creative Commons Attribution 4.0 International License, which permits use, sharing, adaptation, distribution and reproduction in any medium or format, as long as you give appropriate credit to the original author(s) and the source, provide a link to the Creative Commons licence, and indicate if changes were made. The images or other third party material in this article are included in the article's Creative Commons licence, unless indicated otherwise in a credit line to the material. If material is not included in the article's Creative Commons licence and your intended use is not permitted by statutory regulation or exceeds the permitted use, you will need to obtain permission directly from the copyright holder. To view a copy of this licence, visit http://creativecommons.org/licenses/by/4.0/.

References

Chapman, S.: 1943, Magnetism in the Sun's atmosphere. Mon. Not. Roy. Astron. Soc. 103, 117.

Chapman, S., Bartels, J.: 1940, Analysis of the Data, and Physical Theories, Geomagnetism II, Oxford Univ. Press, London.

Dungey, J.M.: 1958, Cosmic Electrodynamics, Cambridge University Press, New York.

Euler, L.: 1769, Principiis Motus Fluidorum. Novi Comentarii Acad. Sci. Petropolitanae 14, 270.

Hoeksema, J.T.: 1985, The solar magnetic field since 1976. UAG-94, WDC-A.

Ivanov, K.G., Kharshiladze, A.F.: 2006, Dynamics of the large-scale open solar magnetic field and its specific features in the zone of the main active longitudes in 2006–2012. *Geomagn. Aeron.* 46, 683.

Kononovich, E.V., Shefov, N.N.: 2013, Certain regularities of solar activity variations during the 11-year cycle. Geomagn. Aeron. 53, 677.

Levine, R.H.: 1978, The relation of open magnetic structures to solar wind flow. *J. Geophys. Res.* **83**, 4193. Levine, R.H., Altschuler, M.D., Harvey, J.W.: 1977a, Open magnetic structures on the sun. *Astrophys. J.* **215**,

Levine, R.H., Altschuler, M.D., Harvey, J.W.: 1977b, Solar sources of the interplanetary magnetic field and solar wind. *J. Geophys. Res.* 82, 1061.

Newkirk, G., Altschuler, M.: 1969, Magnetic fields and the structure of the solar corona. Bull. Am. Astron. Soc. 1, 288.

Ray, E.: 1963, On the motion of charged particles in the geomagnetic field. Ann. Phys. 24, 1.

Romashets, E., Vandas, M.: 2024, Exact alpha-beta mapping of IGRF magnetic field in the ionosphere. J. Geophys. Res. 129, e2023JA032131. DOI.

Romashets, E., Vandas, M., Poedts, S.: 2007, Modeling of the three-dimensional motion of toroidal magnetic clouds in the inner heliosphere. Astron. Astrophys. 466, 357.

Schulz, M., Chen, M.: 2008, Field-line (Euler-potential) model of the ring current. J. Atmos. Solar-Terr. Phys. 70, 482

Sweet, P.A.: 1950, The effect of turbulence on magnetic field. Mon. Not. Roy. Astron. Soc. 110, 69.

Vitinskii, Y.I., Kopetskii, M., Kuklin, G.V.: 1986, Statistics of Spot-Generating Solar Activity, Nauka, Moscow.

Webb, G.M., Hu, Q., Dasgupta, B., Zank, G.P.: 2010, Homotopy formulas for the magnetic vector potential and magnetic helicity: the Parker spiral interplanetary magnetic field and magnetic flux ropes. *J. Geophys. Res.* 115, A10112. DOI.

Wolf, R.A., Spiro, R.W., Sazykin, S., Toffoletto, F.R., Sager, P.L., Huang, T.-S.: 2006, Use of Euler potentials for describing magnetosphere-ionosphere coupling. *J. Geophys. Res.* 111, A07315. DOI.

Zaharia, S.: 2008, Improved Euler potential method for three-dimensional magnetospheric equilibrium. *J. Geophys. Res.* 113, A08221. DOI.

Publisher's Note Springer Nature remains neutral with regard to jurisdictional claims in published maps and institutional affiliations.

